Available online at www.sciencedirect.com

ScienceDirect

Physics Procedia 56 (2014) 515 – 524

Physics Procedia

8th International Conference on Photonic Technologies LANE 2014

Experimental and numerical investigation of an electromagnetic weld pool control for laser beam welding

M. Bachmann[a], V. Avilov[a,b], A. Gumenyuk[a], M. Rethmeier[a,b,*]

[a] *BAM Federal Institute for Materials Research and Testing, Unter den Eichen 87, 12205 Berlin, Germany*
[b] *Institute of Machine Tools and Factory Management, Technical University Berlin, 10587 Berlin, Germany*

- Invited Paper -

Abstract

The objective of this study was to investigate the influence of externally applied magnetic fields on the weld quality in laser beam welding. The optimization of the process parameters was performed using the results of computer simulations. Welding tests were performed with up to 20 kW laser beam power. It was shown that the AC magnet with 3 kW power supply allows for a prevention of the gravity drop-out for full penetration welding of 20 mm thick stainless steel plates. For partial penetration welding it was shown that an 0.5 T DC magnetic field is enough for a suppression of convective flows in the weld pool. Partial penetration welding tests with 4 kW beam power showed that the application of AC magnetic fields can reduce weld porosity by a factor of 10 compared to the reference joints. The weld surface roughness was improved by 50 %.

Peer-review under responsibility of the Bayerisches Laserzentrum GmbH

Keywords: laser beam welding; electromagnetic weld pool support; Hartmann effect; electromagnetic rectification

1. Introduction

The advantages of keyhole mode laser beam welding, such as high welding speed and low heat input, are well known. An especially high weld quality is achieved in PA position full penetration keyhole laser beam welding. The

* Corresponding author. Tel.: +49-30-8104-1559; fax: +49-30-8104-1557 .
E-mail address: michael.rethmeier@bam.de

Peer-review under responsibility of the Bayerisches Laserzentrum GmbH
doi:10.1016/j.phpro.2014.08.006

laser beam forms a narrow weld pool with nearly parallel side walls. During solidification of the weld pool, the longitudinal and transversal shrinkage stress variations along the keyhole axis are much lower than in most other welding technologies. This results in very low buckling and bending of the workpiece (Ready et al. (2001)). Moreover, full penetration welding can suppress the development of the so-called process porosity due to the keyhole instability near its bottom tip, see Seto et al. (2001). However, for full penetration welding of thick metal parts the surface tension cannot completely compensate the hydrostatic pressure in the melt. This can result in sagging of the root side of the weld or even a complete drop-out of the melt when the workpiece thickness is above a threshold.

Both AC and DC magnetic fields can be effectively used to control large amounts of molten metal in many industrial processes, e.g. crystal growth and metal casting. The so-called electromagnetic (EM) processing is widely used and well-known to stabilize the surface of solidifying material, to accelerate (EM stirring) or decelerate (the Hartmann effect) the convection in metal flows to refine the melt from oxide particles and gas bubbles (EM rectification), see e. g. the proceedings of the last EPM (Electromagnetic Processing of Materials) conference 2012.

The idea to use this technology to prevent the gravity drop-out in high power laser beam welding of thick stainless steel plates was developed in Jones et al. (2003) and successfully verified in full penetration welding tests of up to 12 mm thick stainless steel (Avilov et al. (2009)) and 30 mm thick Al-alloy plates (Avilov et al. (2012)).

The numerical investigations in this paper were made with the commercial finite element solver COMSOL Multiphysics 4.2 to get insights into the process zone and a detailed description of the underlying effects as well as to analyze the MHD interactions with the fluid flow and subsequent solidification behavior in the weld pool. Moreover, a simulation allows for an optimization of the process parameters including the amplitude and the frequency of the magnetic field.

2. Physical Background

The interaction between the fluid flow during welding and the applied magnetic fields is due to the Lorentz force

$$\mathbf{F_L} = \mathbf{j} \times \mathbf{B}, \tag{1}$$

where $\mathbf{j}$ and $\mathbf{B}$ are the electric current density and the magnetic flux density. When the applied magnetic field is of oscillatory nature, electric eddy currents develop in the workpiece inside the skin depth which depends on the applied oscillation frequency according to the classical skin effect theory, see Landau et al. (1984):

$$\delta = \left(\pi \mu_0 \sigma f\right)^{-1/2}, \tag{2}$$

with the magnetic permeability in vacuum μ_0, the electric conductivity σ and the frequency f. The time-average of the resulting electromagnetic force is directed against the gravity force. Thus, a drop-out of metal can be suppressed. A further component to the electric current density is due to the movement of the electrically conducting material transverse to the magnetic field:

$$\mathbf{j_u} = \mathbf{u} \times \mathbf{B}. \tag{3}$$

The part of the Lorentz force due to this effect is directed against the melt velocity acting as a braking force. That force is also present for the application of time-invariant magnetic fields and is called Hartmann effect. The strength of the electromagnetic deceleration can be expressed in terms of the Hartmann number:

$$\mathrm{Ha}^2 = \sigma\left(|\mathbf{B}|L\right)^2 / \eta, \tag{4}$$

with the half weld bead width L and the dynamic viscosity η. Schematic illustrations of both effects can be seen in Figure 1.

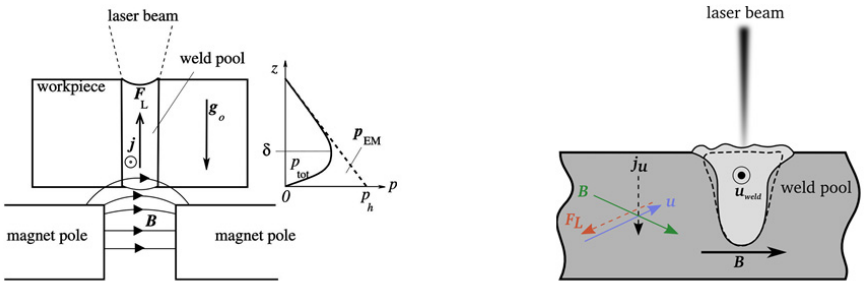

Fig. 1. Schemas of the inductive weld pool support (left) and the Hartmann effect (right) in high power laser beam welding.

The time-averaged Lorentz force is

$$F_{\mathrm{L}}(z)=\frac{B^2}{\mu_0\delta}\exp\left(-\frac{2z}{\delta}\right), \tag{5}$$

where B is the rms-value of the applied magnetic field on the weld pool surface.

An oscillating magnetic field can effectively remove gas bubbles and other non-conducting inclusions from the melt (EM rectification, see e.g. Takahashi et al. (2003)). All non-conductive inclusions (e. g. bubbles or oxide particles) in the melt disturb the ideal profile of the electric current density. As a result, the inclusion is forced to move in the opposite direction of the electromagnetic force F_{L}. Based on the Lenov–Kolin theory (Lenov et al. (1954)) the total EM Archimedes force F_{A} (per unit volume) acting on a small inclusion (smaller than δ) can be written as follows. The Lenov-Kolin factor G_{LK} for spherical bubbles is 0.75.

$$F_{\mathrm{A}}(z)=G_{\mathrm{LK}}F_{\mathrm{L}}V \tag{6}$$

Another EM technology is the stabilization of the weld pool surface (Garnier-Moreau effect). This effect can be explained in terms of the so-called EM contribution to the surface tension. .

$$\gamma_{\mathrm{EM}}=B^2L\,F_{\mathrm{GM}}(\delta/L)/\mu_0 \tag{7}$$

The function F_{GM} is shown in Figure 2.

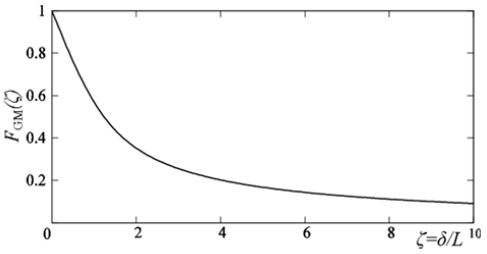

Fig. 2. The form-factor F_{GM} for the EM contribution to the effective surface tension.

The sources of intensive EM stirring in the weld pool are the temperature dependence of the electrical conductivity σ as well as irregularities (edges) of magnet poles and welded parts. Both of these effects can intensify undesirable EM stirring in the weld pool.

3. Numerical simulation of a weld pool support by oscillating magnetic fields

The availability of high power laser systems enables the full-penetration welding of very thick components, e.g. for pressure vessels or power station components. The hydrostatic pressure in the melt can exceed the pressure due to surface tension and results in sagging or even a complete drop-out of the melt, see Figure 3. Experimental results from Avilov et al. (2009) show the possibility of a contactless weld pool support system by oscillating magnetic fields that works in all welding positions. A moderate magnetic flux density of around 141 mT was necessary to compensate a 12 mm melt column of AISI 304 at an oscillation frequency of 3.18 kHz.

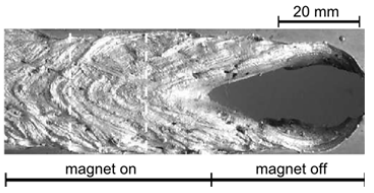

Fig. 3. Full-penetration welding of 30 mm thick AlMg3 with magnetic weld pool support (left) and without (right).

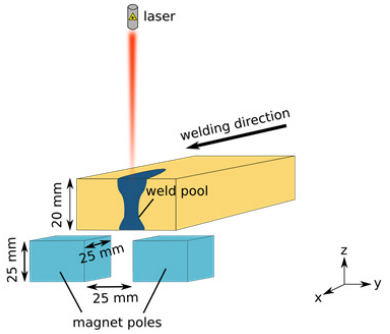

Fig. 4. Setup for the simulation of an electromagnetic weld pool support system.

The solved equation system comprise the Navier-Stokes equations for the fluid dynamics, the energy equation for the temperature distribution and the Maxwell equations to take into account the influence of the arising Lorentz forces on the process variables. The simulations calculate the main physical aspects of the welding process; namely the Marangoni convection at the surfaces, the gravity-driven natural convection and the latent heat of fusion during the local melting and solidification. The material properties depend on the local temperature field.

The keyhole geometry and the workpiece surfaces were fixed in the simulations. Simulating the weld pool support, the pressure differences between the upper and lower surfaces were analyzed to evaluate the degree of compensation of the hydrostatic pressure. The formula apparatus and simulation details can be found in detail in Bachmann et al. (2012), Bachmann et al. (2013) and Bachmann et al. (2014).

The setup for the numerical investigations can be found in Figure 4. The magnetic field is oriented perpendicular to the welding direction. Thus the resulting Lorentz forces are directed mainly in vertical direction acting against the gravitational forces independently of the oscillation cycle phase.

3.1. Aluminum

The simulation results for the full-penetration welding of 20 mm thick aluminum with a welding speed of 0.5 m/min without applied magnetic fields (reference case) as well as with three different magnetic flux densities are shown in Figure 5. The hydrostatic pressure in the reference case is linearly increasing with the depth in the weld pool. Applying a magnetic field tends to lower the pressure differences between the surfaces up to a balance state with nearly no gravity driven drop-out or sagging of melt which was detected at around 70 mT and an oscillation frequency of 450 Hz. According to the Lorentz force distribution, the flow dynamics in the weld pool is only affected in the lower part within the skin depth of the applied magnetic field, see Figure 6. Large-scaled Marangoni vortex formations occur near the surfaces due to the temperature variation of the surface tension. In the lower part of the weld pool, the electromagnetic forces induce a second vortex acting against the Marangoni vortex which indicates a Lorentz force gradient there which is due to the relation of the magnet pole and the length of the molten zone (see Bachmann et al. (2012)). Hence, the weld pool shortens by the applied forces. The magnitudes of the flow

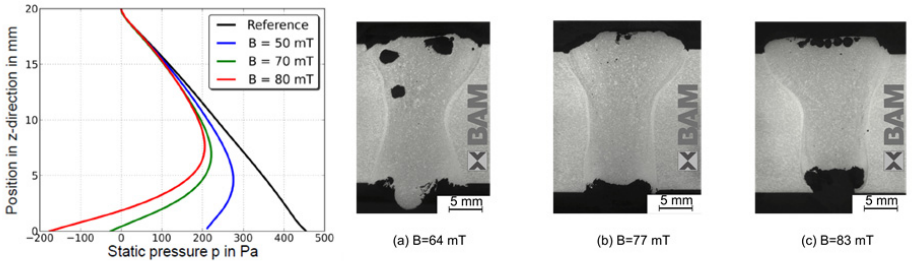

Fig. 5. Left: Static pressure distribution in vertical direction through the weld pool for different magnetic flux densities. The welding speed was 0.5 m/min and the oscillation frequency 450 Hz. Right: Experimental results obtained with a fiber laser (15 kW laser power, focus position -2 mm, 560 µm focal spot diameter, frequency 459 Hz).

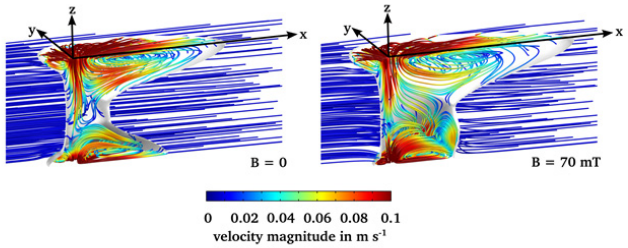

Fig. 6. Velocity streamlines of the reference case and the case of optimal compensation.

velocities in the upper weld pool remain nearly unaffected. Experimentally obtained weld pool macrographs of AlMg3 (Figure 5) show the same trends found in the simulations, namely sagging was avoided and the weld geometry was Y-shaped. A detailed description can be found in Bachmann et al. (2012).

3.2. Stainless steel AISI 304

The same approach as for aluminum was also pursued for 20 mm thick stainless steel AISI 304. In the simulations, the material was assumed to behave ideally non-ferromagnetic. Three different oscillation frequencies were investigated corresponding to skin depths of a quart, a half and the full weld depth. The welding speed was set to 0.4 m/min. Figure 7 shows the pressure and Lorentz force distributions for the reference case and the magnetic support cases. Increasing the frequency produces a steeper Lorentz force and accordingly a steeper pressure gradient in the lower part of the weld pool due to the skin effect. Nevertheless, an optimal control of the hydrostatic pressure

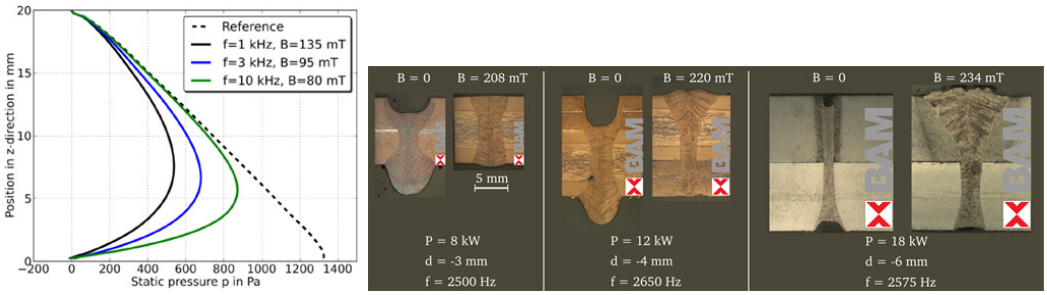

Fig. 7. Left: Static pressure distribution in vertical direction through the weld pool for different magnetic flux densities and oscillation frequencies. The welding speed was 0.4 m/min. Right: Experimental results obtained with a fiber laser (variable laser power, focus position, oscillation frequency and magnetic flux density, 560 µm focal spot diameter) for plate thicknesses of 10 mm, 15 mm and 20 mm.

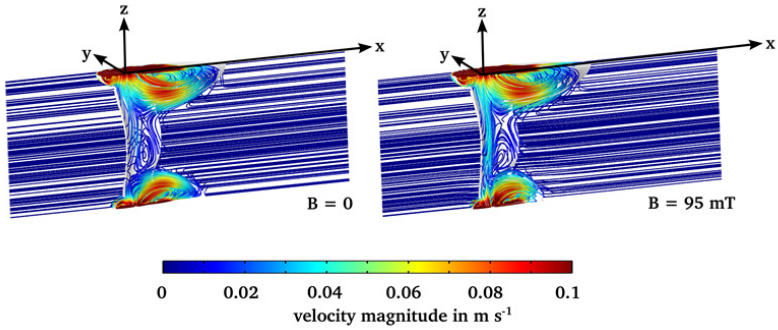

Fig. 8. Velocity streamlines of the reference case and the case of optimal compensation for a frequency of 3 kHz.

in the melt was proven for all frequencies. Increasing the frequency leads to lower magnetic flux densities for the compensation of the 20 mm stainless steel, see Bachmann et al. (2014), which is due to a frequency-dependent relation between the applied magnetic flux density and the resulting Lorentz force.

In comparison to aluminum, stainless steel has a significantly lower thermal conductivity. Therefore, the weld pool length for a similar welding speed is smaller, see Figure 8. The main characteristics of the fluid flow inside the molten pool also just remain the same. Due to the smaller weld pool dimensions at a constant magnet pole geometry, the Lorentz force gradient in the liquid region is smaller compared to aluminum. Therefore, the flow characteristics in the lower part of the weld pool is still similar to that in the upper region outside the penetration depth of the magnetic field when welding with electromagnetic support system. Experimental results for different thicknesses can be seen in Figure 7.

4. Numerical simulation of a weld pool deceleration by steady magnetic fields

Another MHD effect to control unfavorable dynamics in the weld pool especially when welding very thick components associated to severe spattering is called the Hartmann effect. Experimental work in this field in welding was done by Kern et al. (2000) with a CO_2 laser. He observed a distinct smoothing of the weld pool surface and the humping phenomenon was suppressed depending on the polarity of the applied magnetic field. However, the Hartmann number was only around 100. A disk laser was used in the present investigation for the partial penetration welding of aluminum with a keyhole penetration of around 21 mm. Permanent magnets were mounted on both sides of the workpiece to maximize the magnetic flux density in the weld pool, see Figure 9. The numerical model used the standard two equation k-ε turbulence model.

Velocity streamlines for the reference case as well as the case with an applied magnetic field of 0.5 T are shown in Figure 10. In the reference case, the flow characteristics is mainly due to the Marangoni stresses which cause the

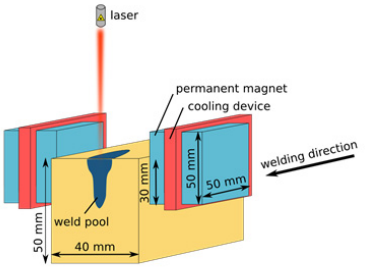

Fig. 9. Setup for the simulation of an electromagnetic weld pool control system.

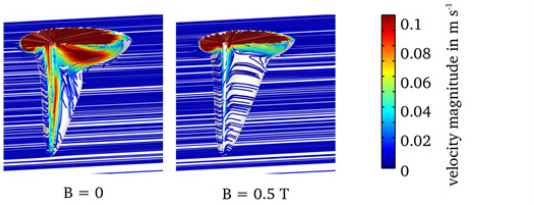

Fig. 10. Velocity streamlines in the weld pool without and with magnetic control for a welding speed of 0.5 m/min.

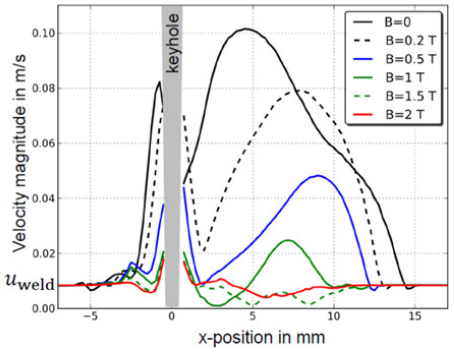

Fig. 11. Flow velocities along the welding direction in the symmetry plane 2 mm below the workpiece surface.

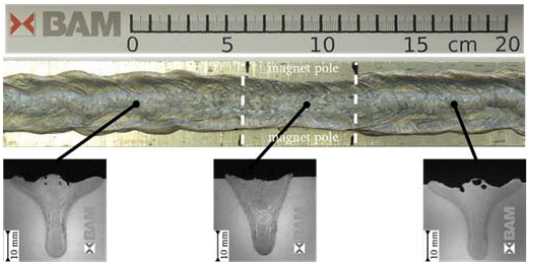

Fig. 12. Experimental results for the welding of AlMg3 with a welding speed of 0.5 m/min without (left and right) and with permanent magnets (500 mT) applied (center). Welds were made with a disk laser (16 kW, focus position -4 mm, 300 µm focal spot diameter, magnetic flux density 0.5 T).

liquid metal to flow from hot regions around the keyhole to the boundary regions. When a magnetic field is applied, the flow velocities in the weld pool are significantly smaller due to the braking nature of the Hartmann effect, see Figure 11. In the depth of the weld pool, the reversal of the flow due to the Marangoni effect is limited to an ever thinner boundary region with increasing magnetic flux density. It was found that a Hartmann number of around 10^4 was necessary for a dissipative influence of the applied magnetic forces (Bachmann et al (2013). Furthermore, the suppression of the flow dynamics leads to a regular V-shape of the weld bead in the simulations and in the experiments as well (Figure 12).

5. Partial penetration laser welding with EM control of the weld pool

In the next two subsections, the results of partial penetration laser beam welding tests of Al alloy components are shown. The first problem of partial penetration laser beam welding is the keyhole-tip instability representing the main source of porosity – gas bubbles leave the keyhole near its tip, see Seto et al. (2001). The second problem is very intensive thermocapillary (Marangoni) convection in the upper part of the weld pool. The surface tension cannot completely suppress oscillations of the weld pool surface and the re-solidified welds show very rough surfaces with large undercuts. Here, AC magnetic fields were used to suppress porosity formation and to stabilize the weld pool surface in bead-on-plate partial penetration laser beam welding of 10 mm thick AlMg3 plates in flat position.

5.1 Experimental set-up

All welding experiments were performed using 4 kW laser beam power. The AC magnet was mounted direct on the welding head of the laser welding optics. The externally applied AC magnetic field was oriented perpendicularly to the welding direction. To prevent optical feed-back the incident angle α of the laser beam was taken to be 18° to the vertical, see Figure 13. The magnet core was made of 0.05 mm thick Fe-Si lamination (microsil). The cross-section of both magnet poles (Fluxtrol A) was 20 mm × 20 mm. The gap between the magnet poles was 20 mm and the distance between the AC magnet and the sample was 2 mm. The shielding gas (argon with a flow rate of 20 l/min) was supplied to the front side of the weld pool.

The main parameters of the laser beam source (TRUMPF Yb:YAG thin disk laser TruDisk 16002, max. beam power 16 kW) are listed in Table 1.

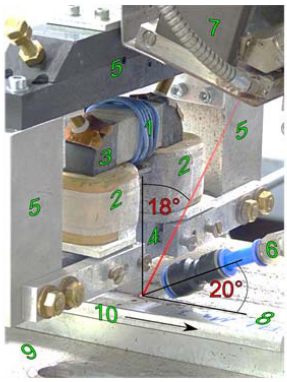

Fig. 13. Experimental setup:
1- primary coil,
2- two secondary coils,
3- ferromagnetic core,
4- magnet poles,
5- assembly elements,
6- shielding gas nozzle,
7- laser welding head,
8- sample,
9- welding table,
10- welding direction.

Table 1. Parameters of the laser beam.

beam power in all welding tests	4 kW
wave length	1.03 µm
beam parameter product	8 mm × mrad
focal length	300 mm
focal spot size	300 µm

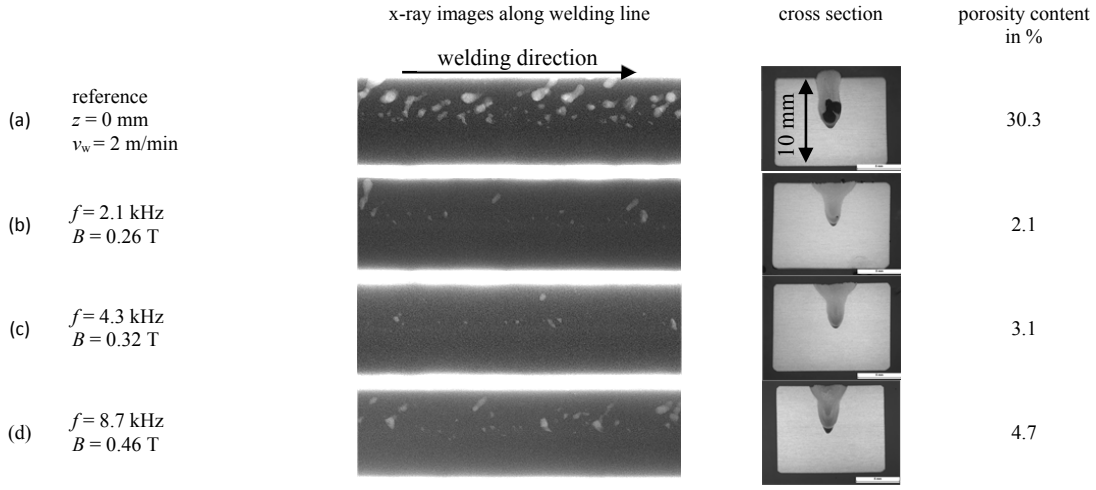

Fig. 14. X-ray side images and cross sections of welds for different parameters of the AC power supply.

5.2 Results and discussion

Figure 14 illustrates the welding tests without and with oscillating magnetic field applied. The reference welds with the focal position set on the surface (z = 0) show a very intensive formation of process porosity. However, this type of pores is quasi-spherical and they are located in the center of the weld pool. Hence, it is expected, that the magnetic field can successfully prevent this type of pores. The amplitude of the magnetic field must be large enough and the skin depth in the order of the penetration depth (around 6 mm).

Figure 14(b)-(d) show x-ray side views of the welds with EM weld pool control as well as metallographic cross sections. Analyses of the cross-sections and the x-ray images show a drastic reduction (more than 90 %) of the weld porosity for an optimal oscillation frequency. The observed effects can be explained in terms of EM Archimedes forces as well as the EM stirring in the weld pool.

Further improvements by the application of the magnetic fields were also observed in terms of the surface quality, see the cross sections in Figure 14 and the measured surface profiles in Figure 15. The usage of AC magnetic fields results in a significant reduction of up to 50 % of the weld surface roughness. Figure 16 shows the surface quality in terms of welding-induced undercuts according to DIN EN ISO 13919-2:2001. Here, a clear reduction is remarkable and the quality level could be improved from group D in the reference case to group B with all oscillation frequencies of the magnetic fields applied.

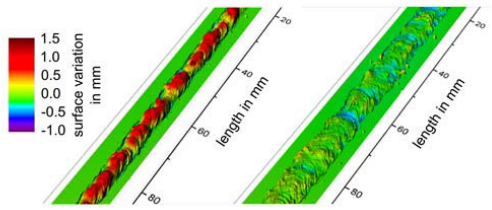

Fig. 15. Weld surface variations for the reference case (left) and case (c) from Figure 14.

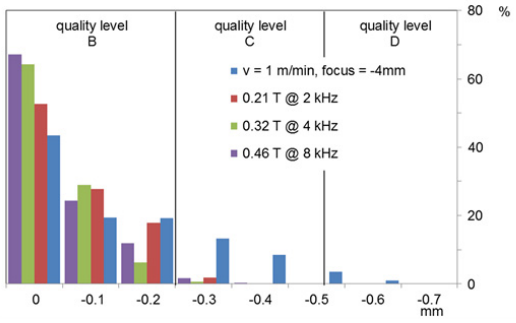

Fig. 16. Histogram of the measured depth on the weld seam surface. Only negative values are considered for undercuts.

6. EM weld pool control for laser beam welding with filler wire

A series of welding tests was performed to demonstrate that the EM weld pool control can also be used for industrial laser beam welding applications with filler wire such as the welding of butt joints of complex non-planar parts. Figure 17 shows the experimental setup, which simulates the joining of a lid to the opening of a container with high quality requirements (leak-proof). Both welded parts are made of AlMgSi0.5 alloy. Due to the risk of hot cracking, the welding of this alloy is only possible with filler material (AlMg4.5Mn, wire with 1.2 mm diameter).

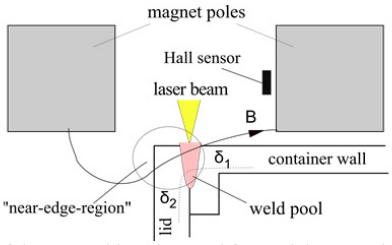

Fig. 17. Scheme of the EM weld pool control for partial penetration welding of the lid to the container wall.

Table 2. Parameters of the EM weld pool control for three welding tests.

weld Nr.	*B*, mT	*f*, kHz	δ(cold),mm	weld dimensions in mm width & depth	
reference	0			4.2	3.2
1	173	1.9	2.1	5.0	2.7
2	225	1.9	2.1	5.0	2.7
3	264	4.0	1.4	5.0	2.7

All welding tests were performed in flat position using an Yb-fiber laser YLR-20000 at 4 kW laser beam power. The inclination angle of the laser beam was taken to be 8° to the vertical, see Figure 13. The diameter of the beam delivery fiber was 0.2 mm. The beam diameter at the focal plane corresponds to 560 µm and the focal length was 350 mm. The focal position was z = -3 mm (under the surface). The shielding gas nozzle (industrial grade argon with a flow rate of 20 l/min) was placed behind the laser beam. The welding velocity and the wire feed rate for all welding tests were taken to be 1.7 m/min and 2.2 m/min, respectively. The gap between the magnet poles was 22.5 mm and the gap between the magnet and the workpiece was 2 mm. Both the focal position of the laser beam and the contact point of the filler wire correspond to the middle of the area located between the magnet poles. For full penetration welding the AC magnet can be placed near the root of the specimen and the filler wire nozzle can be mounted on the welding head on the front side. If the skin-depth is lower than the workpiece width, the AC magnet field does not influence the filler wire. However, for the container closing process there is no access to the interior space of the workpiece. Thus, only partial penetration laser welding process is possible. Both the AC magnet and the filler wire nozzle must be located on the outer side of the container wall. The filler wire nozzle was made of electrically non-conductive material (Teflon) and the filler wire system was electrically disconnected from the workpiece to prevent the excitation of eddy currents.

In Figure 17, B is the rms value of the magnetic flux density measured near the center of the right magnet pole with a Hall sensor, f is the AC frequency and δ is the skin depth in Eq. (2) calculated for cold Al alloy with the electrical conductivity at room temperature $\sigma \approx 30 \cdot 10^6$ Si m^{-1}. Note, that the electrical conductivity of the melt is much lower, i.e. the effective skin-depth in the weld pool can be up to 3 times larger than the values shown in Table 2.

Figure 18 shows x-ray side images and macro sections of three welding tests performed with and without EM weld pool control. A significant reduction in the number of pores and pore size is evident when compared to the corresponding reference cases for all three cases investigated. The last two columns in Table 2 show the width and the depth of the welds. These values were obtained from an

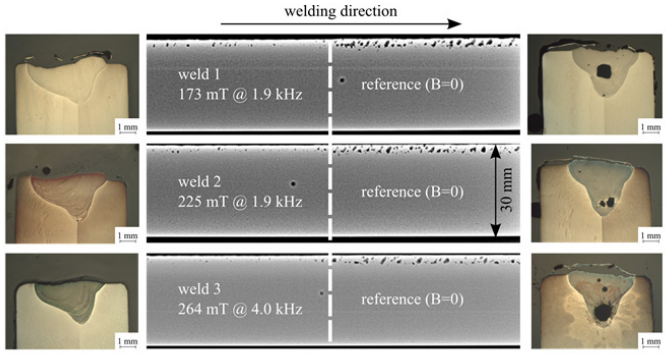

Fig. 18. X-ray side images for three welds listed in Table 2.

analysis of the weld cross-sections. The welds with EM control are wider than their references and their penetration depth becomes smaller. This can be explained by an intensive stirring in the melt due to an inhomogeneous Lorentz force distribution in the weld pool caused by the asymmetric workpiece setup. This effect, in addition to the pore removal, is especially useful for the dilution in the weld material when welding structures with very deep weld beads with filler material. The inhomogeneous Lorentz force distribution is also noticeable by the asymmetric weld macro sections when welding with EM control in Figure 18.

7. Summary & Conclusions

The present investigations reveal that oscillating and steady magnetic fields can have a significant positive effect on the quality as well as the stability of high-power laser beam welding processes of aluminum alloys and stainless steel. The results in this paper point to various EM applications in welding, e.g. the EM weld pool support, the EM braking of the flow velocities, the EM rectification, and EM weld surface improvements that can be used for a variety of industrial applications.

The most decisive quantities for a successful application of EM technologies in welding are the magnetic flux density and, in the case of oscillating magnetic fields, the frequency and the according skin depth. Additionally, the orientation of the applied magnetic fields relative to the workpiece is relevant for the performance of the MHD effects in the weld bead.

Clear improvements in terms of avoiding melt sagging, reducing spattering, decreasing surface roughness, and the reduction of pore content could be demonstrated. Thus, the EM technology could be numerically and experimentally proven to be an appropriate tool for a successful implementation in various welding applications.

Acknowledgements

Financial funding of the DFG (Bonn, Germany) under Grant No. DFG GU 1211/2-1 and the German Allianz Industrie Forschung (AiF), Grant No. 17.265N is gratefully acknowledged.

References

Avilov, V., Gumenyuk, A., Lammers, M., Rethmeier, M., 2012. PA position full penetration high-power laser beam welding of up to 30 mm thick AlMg3 plates using an electromagnetic weld pool support, Sci. Technol. Weld. Joining 17, 128–133.

Avilov, V., Moldovan, R., Berger, P., Graf, T., Mock, D., 2009. Electromagnetic weld pool control by CO2 and YAG disk laser welding of thick stainless steel plates, Proceedings of the 6th International Conference on Electromagnetic Processing of Materials, Dresden.

Bachmann, M., Avilov, V., Gumenyuk, A., Rethmeier, M., 2012. Numerical simulation of full-penetration laser beam welding of thick aluminium plates with inductive support, J. Phys. D: Appl. Phys. 45, 035201.

Bachmann, M., Avilov, V., Gumenyuk, A., Rethmeier, M., 2013. About the influence of a steady magnetic field on weld pool dynamics in partial penetration high power laser beam welding of thick aluminium parts, Int. J. Heat Mass Tran. 60, 309–321.

Bachmann, M., Avilov, V., Gumenyuk, A., Rethmeier, M., 2014. Experimental and numerical investigation of an electromagnetic weld pool support system for high power laser beam welding of austenitic stainless steel, J. Mater. Process Tech. 214, 578–591.

Bojarevics, V., Freibergs, Y., Shilova, E.I., Shcherbinin, E.V., 1989. Electrically Induced Vertical Flows, Kluwer.

Gatzen, M., Tang, Z., Vollertsen, F., 2011. Effect of electromagnetic stirring on the element distribution in laser beam welding of aluminium with filler wire, Physics Procedia 12, 56–65.

Jones, L.P., Aubert, P., Avilov, V., Coste, F., Daenner, W., Jokinen, T., Nightingale, K.R., Wykes, M., 2003. Towards advanced welding methods for the ITER vacuum vessel sectors, Fusion Eng. Des. 69, 215–220.

Kern, M., Berger, P. Hügel, H., 2000. Magneto-Fluid Dynamic Control of Seam Quality in CO2 Laser Beam Welding, Weld. J. 3, 72s–78s.

Landau, L.D., Lifshitz, E.M. 1984 Course of theoretical physics, Vol. 8: Electrodynamics of Continuous Media, Pergamon Press, 460pp.

Lenov, D., Kolin, A. 1954 Theory of electromagnetophoresis (l): Magnetohydrodynamic forces experienced by spherical and symmetrically oriented cylindrical particles, J. Chem. Phys., 22, 683-688.

Moreau, R., 1990. Magnetohydrodynamics, Kluwer, 313pp.

Proceedings 7th International Conference on Electromagnetic Processing of Materials, Beijing, China, 2012.

Ready, J.F., Farson, D.F., Feeley, T. 2001. LIA Handbook of Laser Materials Processing, Laser Institute of America.

Seto, N., Katayama, S., Matsunawa, A., 2001. Porosity formation mechanism and suppression procedure in laser welding of aluminium alloys, Weld. Int. 15, 191–202.

Takahashi, Koichi, Taniguchi, Shoji, 2003. Electromagnetic separation of nonmetallic inclusion from liquid metal by imposition of high frequency magnetic field, ISIJ International, 43, 820–827.